Predicted Variations in Flow Patterns in a Horizontal CVD Reactor

Maria A. Kuczmarski

NASA Lewis Research Center, Cleveland, OH, 44135, USA

Abstract

Expressions in terms of common reactor operating parameters were derived for the ratio of the Grashof number to the Reynolds number, Gr/Re, the ratio of the Grashof to the square of the Reynolds number, Gr/Re^2, and the Rayleigh number, Ra. Values for these numbers were computed for an example horizontal CVD reactor and compared to numerical simulations to gauge their effectiveness as predictors of the presence or absence of transverse and longitudinal rolls in the reactor. Comparisons were made for both argon and hydrogen carrier gases over the pressure range 2-101 kPa. Reasonable agreement was achieved in most cases when using Gr/Re to predict the presence of transverse rolls and Ra to predict the presence of longitudinal rolls. The ratio Gr/Re^2 did not yield useful predictions regarding the presence of transverse rolls. This comparison showed that the ratio of the Grashof number to the Reynolds number, as well as the Rayleigh number, can be used to predict the presence or absence of transverse and longitudinal rolls in a horizontal CVD reactor for a given set of reactor conditions. These predictions are approximate, and care must be exercised when making predictions near transition regions.

key words: flow patterns, CVD, modeling

1. INTRODUCTION

Chemical vapor deposition (CVD) is an important method for depositing solid films from reactive gaseous precursors. It finds applications in many industries, particularly when high purity films are required. The flow patterns inside the reactor can have a significant effect on the properties of the deposited material, making an understanding of such flows crucial to the control of the process. Mathematical models are useful for examining how changes in the reactor's operating parameters affect the flow inside the reactor. The results obtained can be used as a guide to experimental work aimed at attaining material with required characteristics. General purpose commercially available codes greatly ease the work of constructing such models.

Two commonly observed types of flow patterns in horizontal CVD reactors are transverse rolls, which have axes perpendicular to the main flow, and longitudinal rolls, which have their axes parallel to the direction of the main flow [1]. Longitudinal rolls result in a spiral motion of the fluid as it travels down through the reactor. Transverse and longitudinal rolls within the reactor can compromise the uniformity of the deposited material by contributing to local variations in the temperature and species concentrations. In the case where such rolls exist and the Schmidt number, $Sc = \frac{\nu}{D_{i,m}}$, (where ν is the kinematic viscosity and $D_{i,m}$ is the diffusivity of species i in the mixture), is much greater than one, any particles that form in the gas phase are more likely to grow if caught in these rolls, since their residence time in the reactor is increased. Eliminating such flow patterns should increase the uniformity of the flow, thereby contributing to increased deposition uniformity. Changes in the flow pattern can be accomplished by altering the reactor operating conditions.

Two-dimensional flow calculations and flow visualization experiments have shown that for small values of the Reynolds number, Re, transverse rolls occurred when the ratio of the Grashof number (Gr) to the Reynolds number, Gr/Re, was greater than a critical value that was a weak function of the dimensionless temperature difference, $r_T = \frac{T_{sus} - T_{in}}{T_{in}}$, where T_{sus} is the temperature of the heated susceptor and T_{in} is the temperature at the reactor inlet [2]. It was concluded that for Re < 10, Gr/Re should be kept well below 60 to prevent transverse rolls. Another study used two-dimensional simulations verified by experimental results to estimate the extent of transverse rolls (also referred to as recirculation) in a horizontal reactor [3]. This study determined that no transverse rolls should be expected for Gr/Re < 24. For 24 < Gr/Re < 75, the simulations showed areas of low velocity or nearly stagnant regions of gas that were replaced by transverse rolls in the same areas when Gr/Re > 75. Another computational study found that transverse rolls were always absent when Gr/Re < 100 for $1\times10^{-3} < Re \leq 4$ [1]. The Grashof and Reynolds numbers were computed using fluid properties at the inlet conditions. These criteria yielded good agreement with reported experimental observations.

Some researchers have suggested the use of Gr/Re^n to determine the presence of transverse rolls, where n =1 for small Reynolds numbers and n=2 for larger Reynolds numbers. Transverse rolls were found to occur when Gr/Re^2 was greater than some critical value which depended on the dimensionless temperature difference, as defined above [2]. This criteria applied for $Re \geq 8$. In another study [1], transverse rolls were not present when $Gr/Re^2 < 25$ for $4 \leq Re < 100$, with the Grashof and Reynolds numbers computed using fluid properties at the inlet conditions. However, a number of other studies [3-6] have found that Gr/Re^2 is not reliable in describing the flow in a horizontal reactor.

The Rayleigh number, Ra, may be interpreted as the ratio of the thermal flux by free

convection to that by diffusion. It characterizes the convective state of an enclosed gas subjected to a destabilizing temperature gradient, such as a heated bottom and cold upper wall [7]. This is often the situation in horizontal CVD reactors with water-cooled walls and a heated deposition surface. The Rayleigh number has been used to predict the onset of longitudinal rolls in the flow. Longitudinal rolls have been found to appear for Ra >1708 [2,8].

In this study, expressions for Gr/Re^n, n = 1 and 2, were derived in terms of common reactor operation parameters. Values for these ratios were then computed for an example reactor for two carrier gases, argon and hydrogen, at pressures in the range 2-101 kPa, and predictions were made as to the pressure at which transverse rolls should and should not be present. A similar analysis was carried out using values of Ra, from an expression in terms of reactor operation parameters, to determine the pressures at which longitudinal rolls would and would not be present. These predictions were then compared to a numerical simulation of the flow in the sample reactor, with particular attention paid to the flow over the deposition surface.

2. ANALYSIS OF SYSTEM

While dimensionless numbers cannot provide detailed information regarding a process as complex as CVD, they can provide useful information on the relative magnitudes of various effects. Dimensionless numbers are usually expressed in terms of viscosity, thermal conductivity, heat capacity, and density, which are not the parameters usually controlled in a CVD reactor. Expressions for some dimensionless numbers useful in CVD analysis have been derived in terms of parameters that would normally be controlled in a CVD reactor [9]. These expressions were obtained by assuming ideal gas behavior (a good assumption at the relatively high temperatures and low pressures used for CVD), and estimation techniques for viscosity,

thermal conductivity, and heat capacity based on kinetic theory. From this analysis, the Grashof number, which may be interpreted as the ratio of the momentum flux by free convection to that by diffusion, may be expressed as:

$$Gr = 2.031\times10^{3} g(M\sigma^{4}\Omega^{2})(L^{3})\left(\frac{\Delta TP^{2}}{T^{4}}\right) \quad (1)$$

When the gravitational constant, g, is equal to 9.8 m/s, equation (1) becomes:

$$Gr = 1.9903\times10^{4}(M\sigma^{4}\Omega^{2})(L^{3})\left(\frac{\Delta TP^{2}}{T^{4}}\right) \quad (2)$$

where: M = molecular weight (kg/kgmoles)

σ = hard sphere diameter (angstroms)

Ω = collision integral (dimensionless)

L = characteristic length (m)

ΔT = characteristic temperature difference (K)

P = pressure (Pa)

T = temperature (K)

The Reynolds number may be expressed as [9]:

$$Re = 3.747\times10^{5}\left(\frac{\sigma^{2}\Omega}{M^{0.5}}\right)\left(\frac{L}{A_{cs}}\right)\left(\frac{\dot{m}}{T^{0.5}}\right) \quad (3)$$

where: σ = collision diameter (angstroms)

Ω = collision integral (dimensionless)

M = molecular weight (kg/kgmole)

L = characteristic length (m)

A_{cs} = cross-sectional area (m^2)

$\dot{m}$ = mass flow rate (kg/s)

T = temperature (K)

By combining equations (2) and (3), an expressions for Gr/Re and Gr/Re^2 may be obtained:

$$\frac{Gr}{Re} = 5.312\times10^{-2}(M^{1.5}\sigma^2\Omega)(L^2A_{cs})\left(\frac{\Delta TP^2}{\dot{m}T^{3.5}}\right) \tag{4}$$

$$\frac{Gr}{Re^2} = 1.418\times10^{-7}(M^2)(LA_{cs}^2)\left(\frac{\Delta TP^2}{\dot{m}^2T^3}\right) \tag{5}$$

where: M = molecular weight (kg/kgmole)

σ = collision diameter (angstroms)

Ω = collision integral (dimensionless)

L = characteristic length (m)

A_{cs} = cross-sectional area (m^2)

ΔT = characteristic temperature difference (K)

P = pressure (Pa)

$\dot{m}$ = mass flow rate (kg/s)

T = temperature (K)

The collision integral, Ω , is a function of the dimensionless temperature, $\frac{k_B T}{\varepsilon}$, as shown in Figure 2 [10]:

The Rayleigh number, which may be interpreted as the ratio of the thermal flux by free convection to that by diffusion, characterizes the convective state of an enclosed gas subjected to a destabilizing temperature gradient, such as a heated bottom and cold upper wall [2, 7, 8]. This is often the situation in horizontal CVD reactors with water-cooled walls and a heated deposition surface. Longitudinal rolls have been found to appear for Ra >1708 [2]. The Rayleigh number for a monatomic gas may be expressed as [9]:

$$Ra = 1.354\times10^{3} g(M\sigma^{4}\Omega^{2})(L^{3})\left(\frac{\Delta TP^{2}}{T^{4}}\right) \quad \text{(monatomic gas)} \qquad (6)$$

When g = 9.8 m/s, equation (6) becomes:

$$Ra = 1.3267\times10^{4}(M\sigma^{4}\Omega^{2})(L^{3})\left(\frac{\Delta TP^{2}}{T^{4}}\right) \quad \text{(monatomic gas)} \qquad (7)$$

The Rayleigh number for a diatomic gas may be expressed as [9]:

$$Ra = 1.402\times10^{3} g(M\sigma^{4}\Omega^{2})(L^{3})\left(\frac{\Delta TP^{2}}{T^{4}}\right) \quad \text{(diatomic gas)} \qquad (8)$$

When g = 9.8 m/s, equation (8) becomes:

$$Ra = 1.3739\times10^{4}(M\sigma^{4}\Omega^{2})(L^{3})\left(\frac{\Delta TP^{2}}{T^{4}}\right) \quad \text{(diatomic gas)} \qquad (9)$$

The constanst in equations (1) through (9) depend upon the units used for the other variables, so care must be taken when using these equations that all variables are in the specified units.

As an estimate of the temperature in the reactor, the following equation is suggested:

$$T = \frac{T_{sub} + T_{wall}}{2} \tag{10}$$

where: T_{sub} = substrate surface temperature (K)

T_{wall} = reactor wall temperature (K)

The temperature difference can be expressed as:

$$\Delta T = T_{sub} - T_{wall} \tag{11}$$

where: T_{sub} = substrate surface temperature (K)

T_{wall} = reactor wall temperature (K)

Since the main area of interest in a CVD reactor is the deposition surface, equations (10) and (11) should be reasonable estimates of conditions above the surface.

The entrance effects in horizontal reactors may be estimated from the following expressions [7]:

$$x_h = 0.04hRe \qquad \text{(hydrodynamic entrance length)} \tag{12}$$

$$x_T = 0.4hPrRe \qquad \text{(thermal entrance length)} \tag{13}$$

where: x_h = hydrodynamic entrance length (m)

x_T = thermal entrance length (m)

h = channel height (m)

Re = Reynolds number (dimensionless)

Pr = Prandtl number (dimensionless)

In this study, the characteristic length, L, has been chosen to be the channel height. Equations (12) and (13) then become:

$$x_h = 0.04LRe \qquad \text{(hydrodynamic entrance length)} \qquad (14)$$

$$x_T = 0.4LPrRe \qquad \text{(thermal entrance length)} \qquad (15)$$

The Prandtl number may be expressed as:

$$Pr = \frac{\mu C_P}{k} \qquad (16)$$

where: μ = Newtonian viscosity (kg/m s)

Cp = constant pressure heat capacity (J/kg K)

k = thermal conductivity (W/m K)

Using estimation methods for viscosity, heat capacity, and thermal conductivity [9], the Prandtl number is found to be approximately 0.67 for a monatomic gas and 0.69 for a diatomic gas. Equations (15) then becomes:

$$x_T = 0.268LRe \quad \text{(thermal entrance length - monatomic gas)} \tag{17}$$

$$x_T = 0.276LRe \quad \text{(thermal entrance length - diatomic gas)} \tag{18}$$

Equation (14) for the hydrodynamic entrance length applies to an isothermal channel of height L. This entrance length will be somewhat longer for the non-isothermal case used in this study [7]. Equation (15), and, therefore, equations (17) and (18), apply to a horizontal parallel-plate reactor heated from below [7], and should, therefore, be applicable to this study.

3. MODEL

In this study, a 0.515 m long reactor with a 0.0508 m square cross-section was used. A diagram of the modeled reactor is shown in Figure 1. The model has been described in detail previously [11]. Some changes were made to this model for this paper. Since the flow patterns alone were of interest for this study, no chemical reactions were included. Radiation heat transfer was added to the model. The susceptor temperature no longer remains constant, but varies. A constant volumetric heat rate of 1.53×10^8 W/m^3 was specified at the susceptor surface, resulting in a maximum temperature of 1823 K. The inlet volumetric flow rate was increased from 1.2×10^{-5} to 2.2x10-5 m^3/s to more accurately match experimental conditions that have been used in this reactor.

Axial and transverse velocities of zero were specified at the surface of the susceptor, the quartz support, and the reactor walls. The inlet and reactor walls were maintained at a constant temperature of 280 K. The temperature distribution in the quartz support was calculated using the thermophysical properties of quartz. Pressures ranging from 2 kPa to 101 kPa were modeled. The inlet molar flow rate was held fixed as the pressure was varied, resulting in an increase in the inlet velocity as the pressure was lowered.

4. RESULTS AND DISCUSSION

The properties of argon and hydrogen used for this analysis are shown in Table 1, with system conditions are shown in Table 2. The characteristic length was chosen to be the distance between the susceptor surface and the top reactor wall. Equation (14) was used to calculate the hydrodynamic entrance length for both argon and hydrogen carrier gases. Equation (17) was used to calculate the thermal entrance length for an argon carrier gas, and equation (18) was used to calculate the thermal entrance length for a hydrogen carrier gas. Since there seems to be some disagreement in the literature as to which ratio is appropriate for describing flow in a horizontal reactor, the Gr/Re and Gr/Re^2 values for both argon and hydrogen carrier gases were calculated to determine which ratio best described the presence or absence of transverse rolls in the reactor modeled for this work. The values computed for Gr/Re, Gr/Re^2, and Ra are given in Table 3 for argon and Table 4 for hydrogen. Equation (4) was used to compute Gr/Re for both gases, equation (5) was used to compute Gr/Re^2 for both gases, equation (7) was used to compute Ra for argon, and equation (9) was used to compute Ra for hydrogen. The computer program FLUENT was used for the simulations [12]. Velocity vectors were used to visualize transverse rolls, and these vectors were scaled differently for each case for clarity. Streaklines (massless particle trajectories) were used to visualize the longitudinal rolls in the reactor predicted by the computational model. Particles were introduced into the reactor at a height of four centimeters from the bottom of the reactor, which is just above the plane of the deposition surface, and the trail of these particles as they followed the flow was recorded.

The hydrodynamic entrance length was found to be about 0.03 meters for an argon carrier gas and about 0.004 meters for a hydrogen carrier gas. The velocity profiles will be changing over a larger portion of the deposition surface when argon is used as a carrier gas compared to hydrogen. In the sample reactor used in the simulations, the velocity profiles will

be changing over about the first third of the susceptor. The thermal entrance length was found to be about 0.19 meters for an argon carrier gas and about 0.025 meters for a hydrogen carrier gas. When an argon carrier gas is used, the temperature profiles will be changing over the entire length of the deposition surface examined in this study. The temperature profiles will only be changing over about the first third of the deposition surface when hydrogen is used as the carrier gas. With such a large thermal entrance length for argon, large axial temperature variations will likely occur over the deposition surface, raising the question as to whether dimensionless numbers can accurately predict flow patterns for this carrier gas. As discussed later, predictions from these numbers proved valid for argon.

Since the inlet molar flow rate was held constant, the Reynolds number remained the same for each gas even as the pressure was varied. For an argon carrier gas, the Reynolds number was 30. For a hydrogen carrier gas, the Reynolds number was 4. The values for Gr/Re were plotted for both carrier gases in Figure 3. From these plots, the approximate pressures corresponding to critical values for the dimensionless numbers can be determined. Using the criteria from [3], no transverse rolls should exist for $Gr/Re < 24$, while transverse rolls should exist for $Gr/Re > 75$. From the plots of Gr/Re versus pressure in Figure 3a this implies that no transverse rolls should exist for an argon carrier gas at pressures less than about 26 kPa, while transverse rolls should exist at pressures above about 49 kPa. From Figure 3b, no transverse rolls should exist for a hydrogen carrier gas at pressures less than about 67 kPa. A value of Gr/Re greater than 75 is not reached for hydrogen over the pressure range examined here. The computational simulation results, as shown by velocity vectors in Figures 5-10, agree with these predictions. For both carrier gases, transverse rolls begin to be seen at the next highest pressure examined above the pressure determined to be the limit below which transverse rolls should not occur.

The ratio Gr/Re^2 did not yield useful predictions in this study. The values of this ratio at each pressure were the same for argon and hydrogen carrier gases. A plot of Gr/Re^2 versus pressure is shown in Figure 4. From [1], no transverse rolls should exist when $Gr/Re^2 < 25$

when $4 \leq Re < 100$. Both argon and hydrogen carrier gases had Reynolds numbers within this range at all pressures examined, although hydrogen's value was right on the lower limit. Both argon and hydrogen have values of Gr/Re^2 below 25 at all pressures examined, yet transverse rolls existed in the simulations.

As mentioned previously, longitudinal rolls should exist for $Ra > 1708$. As seen from Figure 11, the pressure corresponding to this Rayleigh number is about 54 kPa for an argon carrier gas; the pressure for hydrogen corresponding to this critical Rayleigh value was not reached in the pressure range examined. The computational model results, as shown in Figures 12-17, agree with these predictions, except for hydrogen at 101 kPa, where longitudinal rolls are clearly present. Some waviness in the flow above the deposition surface is observed for the argon carrier gas at a pressure of 40 kPa and for a hydrogen carrier gas at a pressure of 80 kPa, but well-developed longitudinal rolls are still not present.

There are errors associated with the approximations used to obtain equations (7) and (9) [9]; however, these errors are not large enough to result in the order of magnitude difference which would be necessary for the hydrogen carrier gas at 101 kPa to reach critical Rayleigh number. The critical Rayleigh number of 1708 has been obtained for a Boussinesq fluid between parallel plates of constant temperature, the bottom plate at a higher temperature than the top one [8, 13, 14]. The Boussinesq approximation assumes a constant-property fluid, except for density in the gravitational term of the momentum equation, where it assumes a simplified equation of state to approximate the density difference [15]. In the simulated CVD reactor, the fluid properties were variable with temperature, and the susceptor surface (the "bottom wall") although at a higher temperature than the top wall, was not at a constant temperature. The reactor also had a finite length and sidewalls. All of these differences could have contributed to the difference between the predictions regarding longitudinal rolls at 101 kPa for hydrogen and the simulation results. In addition, dimensionless numbers must be calculated from conditions at a particular location, despite the fact that these conditions can

change greatly throughout the reactor. Therefore, these numbers can only provide us an approximate picture of the complex conditions inside a CVD reactor.

5. CONCLUSIONS

The ratio of the Grashof number to the Reynolds number, Gr/Re, has been found to be useful for predicting the pressures at which transverse rolls will be present in a horizontal CVD reactor. Predictions made from the values of this ratio agreed with those from a numerical simulation of a CVD reactor for argon and hydrogen carrier gases over the pressure range 2-101 kPa. The ratio Gr/Re2 was not found to be useful in predicting the pressures at which transverse rolls will be present in a horizontal CVD reactor.

The Rayleigh number, Ra, was found to be useful for predicting the pressure at which longitudinal rolls will be present in a horizontal CVD reactor. Predictions made from the values of this number agreed with numerical simulations of a horizontal CVD reactor for the carrier gases argon and hydrogen over the pressure range 2-101 kPa. The only exception was a hydrogen carrier gas at 101 kPa. The calculated value of the Rayleigh number predicted that longitudinal rolls would not be present; however, the numerical simulation clearly showed that such rolls were present. It must be remembered that the critical value of 1708 for the Rayleigh number used in predicting the presence of longitudinal rolls was derived for a set of conditions that are usually not met in a CVD reactor. This could at least partially explain the discrepancy between the prediction from the Rayleigh number and the numerical simulations at 101 kPa. Also, dimensionless numbers are calculated from conditions at a specific location, despite the fact that these conditions can vary greatly throughout the reactor. In such situations, dimensionless numbers cannot provide an exact description of a CVD reactor, and care must be used in interpreting the predictions obtained from them.

NOTATION

Symbol	Description	Units
A_{cs}	cross-sectional area	m^2
C_p	constant pressure heat capacity	J/kg K
Dim	diffusivity of species i in a mixture	m^2/s
g	gravitational constant	m/s^2
h	channel height	m
k	thermal conductivity	W/m K
k_B	Boltzmann constant	J/ K
Gr	Grashof number	dimensionless
L	characteristic length	m
$\dot{m}$	mass flow rate	kg/s
M	molecular weight	kg/kgmoles
P	pressure	Pa
Pr	Prandtl number	dimensionless
r_T	dimensionless temperature difference	dimensionless
Ra	Rayleigh number	dimensionless
Re	Reynolds number	dimensionless
Sc	Schmidt number	dimensionless
T	temperature	K
T_{sub}	substrate surface temperature	K
T_{wall}	reactor wall temperature	K
ΔT	characteristic temperature difference	K
x_h	hydrodynamic entrance length	m
x_t	thermal entrance length	m

α	thermal diffusivity	m^2/s
ε	characteristic energy of interaction between molecules	J
μ	Newtonian viscosity	kg/m s
σ	hard sphere diameter	angstroms
ν	kinematic viscosity	m^2/s
Ω	collision integral	dimensionless

6. REFERENCES

1. N.K. Ingle, T.J. Mountziaris, "The Onset of Transverse Recirculation During Flow of Gases in Horizontal Ducts with Differentially Heated Lower Walls," J. Fluid Mech., 277, 249-269, 1994.
2. E.P. Visser, C.R. Kleijn, C.A.M. Govers, C.J. Hoogendoorn, L.J. Giling, "Return Flows in Horizontal MOCVD Reactors Studied with the Use of TiO2 Particle Injection and Numerical Calculations," J. Cryst. Growth, 94, 929-946, 1989.
3. R.J. Field, "Simulations of Two-Dimensional Recirculating Flow Effects in Horizontal MOVPE," J. Cryst. Growth, 87, 739-760, 1989.
4. L.J. Giling, "Gas Flow Patterns in Horizontal Epitaxial Reactor Cells Observed by Interference Holography," J. Electrochem. Soc., 129 (3), 634-644, 1982.
5. K-C. Chiu, F. Rosenberger, "Forced Versus Free Convection in Horizontal CVD Reactors," Proceedings of the Tenth International Conference on Chemical Vapor Deposition-1987, editor G.W. Cullen, The Electrochemical Society, Proceedings 87-8, 175-180.
6. J. Vand de Ven, G.M.J. Rutten, M.J. Raaijmakers, L.J. Giling, "Gas Phase Depletion and Flow Dynamics in Horizontal MOCVD Reactors," J. Crystal Growth, 76, 352-372, 1986.
7. G.H. Westphal, "Convective Transport in Vapor Growth Systems," J. Cryst. Growth, 65, 105-123, 1983.
8. K.S. Gage, W.H. Reid, "The Stability of Thermally Stratified Plane Poiseuille Flow," J. Fluid Mech., 33, 21-32, 1968.
9. M.A. Kuczmarski, "Dimensionless Numbers Expressed in Terms of Common CVD Parameters," submitted JCVD, 1997.
10. J.O. Hirschfelder, C.F. Curtiss, R.B. Bird. Molecular Theory of Gases and Liquids. New York: John Wiley & Sons, 1954.
11. M. A. Kuczmarski, "Analysis of Transport in a CVD Silicon Carbide Deposition Reactor," JCVD, 2, 20-41, 1993

12. FLUENT is a computer program for modeling fluid flow, heat transfer, and chemical reactions, from Fluent, Inc., Lebanon, NH, 03766

13. J.W. Deardorff, "Gravitational Instability between Horizontal Plates with Shear," Physics of Fluids, 8(6), 1027-1030, 1965.

14. G.J. Hwang, K.C. Cheng, "Convective Instability in the Thermal Entrance Region of a Horizontal Parallel-Plate Channel Heated from Below," J. Heat Transfer, 95, 72-77, 1973.

15. W.M. Kays, M.E. Crawford. Convective Heat and Mass Transfer. New York: McGraw-Hill, Inc., 1993, p. 398.

16. R. B. Bird, W. E. Stewart, E. N. Lightfoot. Transport Phenomena. New York: John Wiley & Sons, 1960.

Table 1: Properties of argon and hydrogen at T = 1051.5 K [16]

Parameter	Argon Value	Hydrogen Value	Units
M	39.944	2.016	kg/kgmoles
σ	3.418	2.915	angstroms
ε/k	124	38	K
Ω	0.846	0.710	dimensionless

Table 2: System Conditions Used for Analysis

Parameter	Value	Units
L	0.0218	m
A_{cs}	1.11×10^{-3}	m^2
Δ T	1543	K
T	1051.5	K
$\dot{m}_{argon}$	8.693×10^{-5}	kg/s
$\dot{m}_{hydrogen}$	4.387×10^{-6}	kg/s

Table 3: Values for Gr/Re, Gr/Re^2, and Rayleigh numbers at various pressures: argon carrier gas (Re = 30)

Pressure (kPa)	Gr/Re	Gr/Re^2	Ra
2	$1x10^{-1}$	$4x10^{-3}$	$3x10^{+0}$
20	$1x10^{+1}$	$4x10^{-1}$	$3x10^{+2}$
40	$5x10^{+1}$	$2x10^{+0}$	$1x10^{+3}$
60	$1x10^{+2}$	$4x10^{+0}$	$2x10^{+3}$
80	$2x10^{+2}$	$7x10^{+0}$	$4x10^{+3}$
101	$3x10^{+2}$	$1x10^{+1}$	$7x10^{+3}$

Table 4: Values for Gr/Re, Gr/Re^2, and Rayleigh numbers at various pressures: hydrogen carrier gas (Re = 4)

Pressure (kPa)	Gr/Re	Gr/Re^2	Ra
2	$2x10^{-2}$	$4x10^{-3}$	$5x10^{-2}$
20	$2x10^{+0}$	$4x10^{-1}$	$5x10^{+0}$
40	$7x10^{+0}$	$2x10^{+0}$	$2x10^{+1}$
60	$2x10^{+1}$	$4x10^{+0}$	$5x10^{+1}$
80	$3x10^{+1}$	$7x10^{+0}$	$8x10^{+1}$
101	$5x10^{+1}$	$1x10^{+1}$	$1x10^{+2}$

Figure 1: CVD reactor used in model. All dimensions in meters.

Figure 2: Collision integral for viscosity and thermal conductivity calculations as a function of dimensionless temperature for the range: a) $0 < \frac{k_B T}{\varepsilon} < 10$; b) $10 < \frac{k_B T}{\varepsilon} < 400$.

Figure 3: Gr/Re versus pressure for: a) argon; b) hydrogen

Figure 4: Gr/Re^2 versus pressure for argon and hydrogen. The values of this ratio were the same for both gases.

Figure 5: Velocity vectors showing transverse rolls at 2 kPa for : a) argon; b) hydrogen. Flow enters from the left.

Figure 6: Velocity vectors showing transverse rolls at 20 kPa for: a) argon; b) hydrogen. Flow enters from the left.

Figure 7: Velocity vectors showing transverse rolls at 40 kPa for: a) argon; b) hydrogen. Flow enters from the left.

Figure 8: Velocity vectors showing transverse rolls at 60 kPa for: a) argon; b) hydrogen. Flow enters from the left.

Figure 9: Velocity vectors showing transverse rolls at 80 kPa for: a) argon; b) hydrogen. Flow enters from the left.

Figure 10: Velocity vectors showing transverse rolls at 101 kPa for : a) argon; b) hydrogen. Flow enters from the left.

Figure 11: Ra versus pressure for: a) argon; b) hydrogen

Figure 12: Streaklines showing longitudinal rolls at 2 kPa for : a) argon; b) hydrogen. Flow enters from the left.

Figure 13: Streaklines showing longitudinal rolls at 20 kPa for: a) argon; b) hydrogen. Flow enters from the left.

Figure 14: Streaklines showing longitudinal rolls at 40 kPa for: a) argon; b) hydrogen. Flow enters from the left.

Figure 15: Streaklines showing longitudinal rolls at 60 kPa for: a) argon; b) hydrogen. Flow enters from the left.

Figure 16: Streaklines showing longitudinal rolls at 80 kPa for: a) argon; b) hydrogen. Flow enters from the left.

Figure 17: Streaklines showing longitudinal rolls at 101 kPa for a) argon; b) hydrogen. Flow enters from the left.

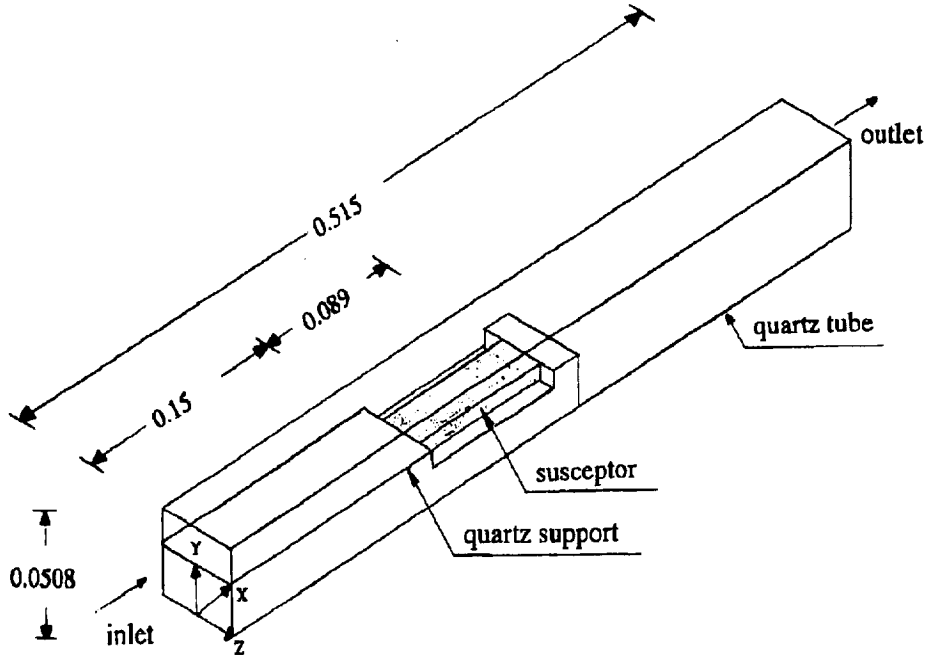
outlet
0.515
0.089
0.15
quartz tube
susceptor
quartz support
0.0508
Y
X
Z
inlet

Figure 1

a)

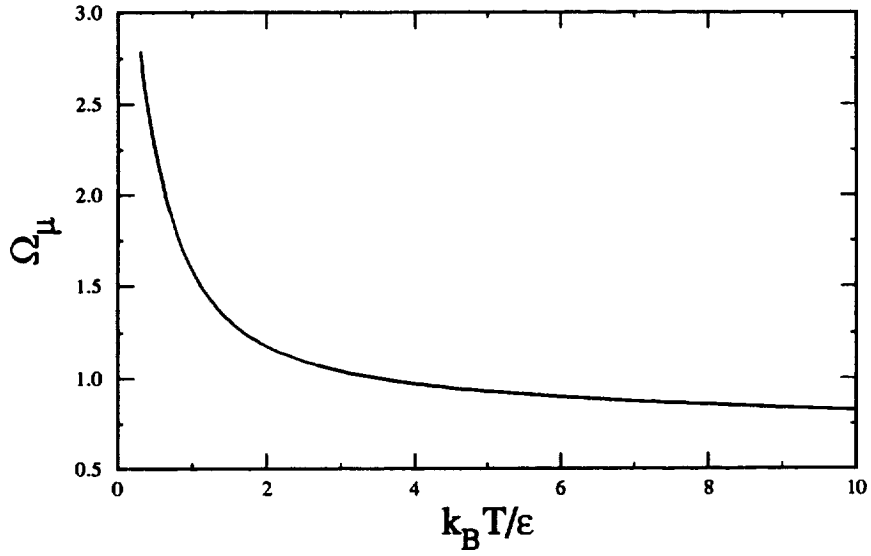
3.0
2.5
2.0
1.5
1.0
0.5
Ω_1^*
0
2
4
6
8
10
k_BT/ε

b)

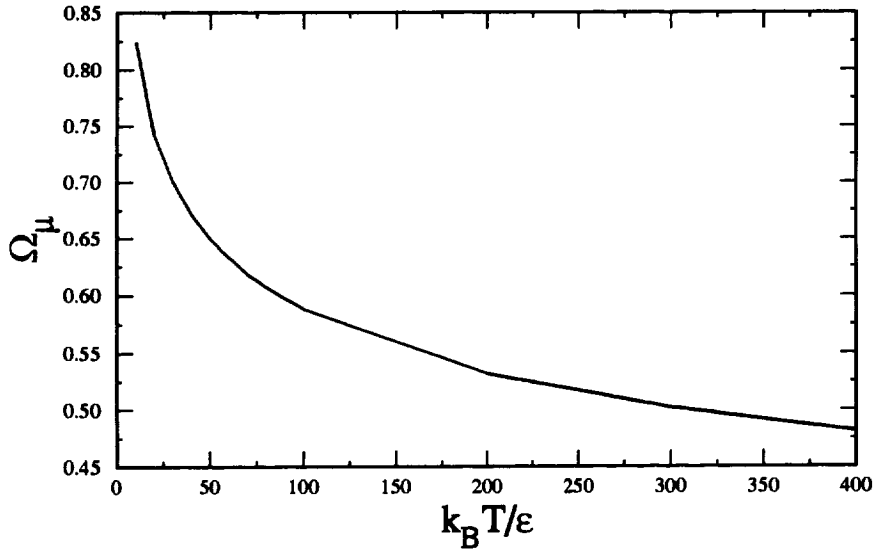
0.85
0.80
0.75
0.70
0.65
0.60
0.55
0.50
0.45
Ω_1^*
0
50
100
150
200
250
300
350
400
k_BT/ε

Figure 2

a)

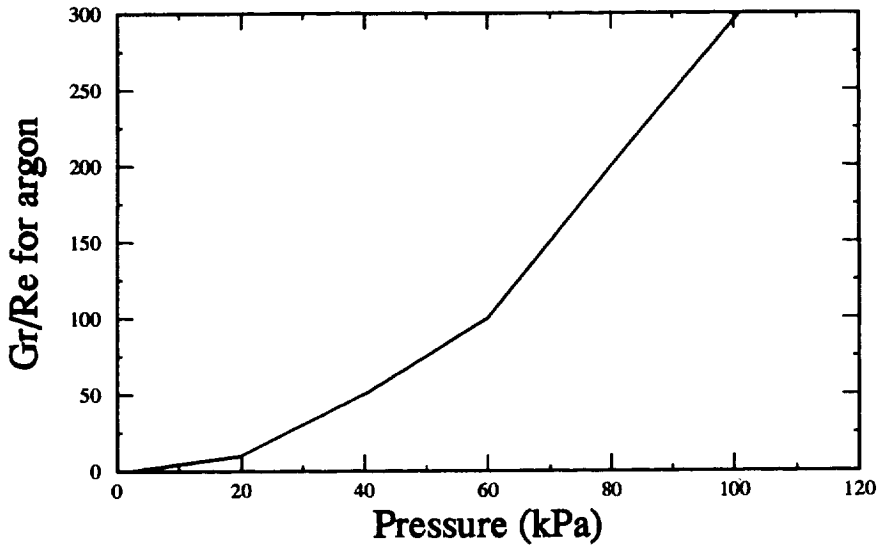
Gr/Re for argon
300
250
200
150
100
50
0
0
20
40
60
80
100
120
Pressure (kPa)

b)

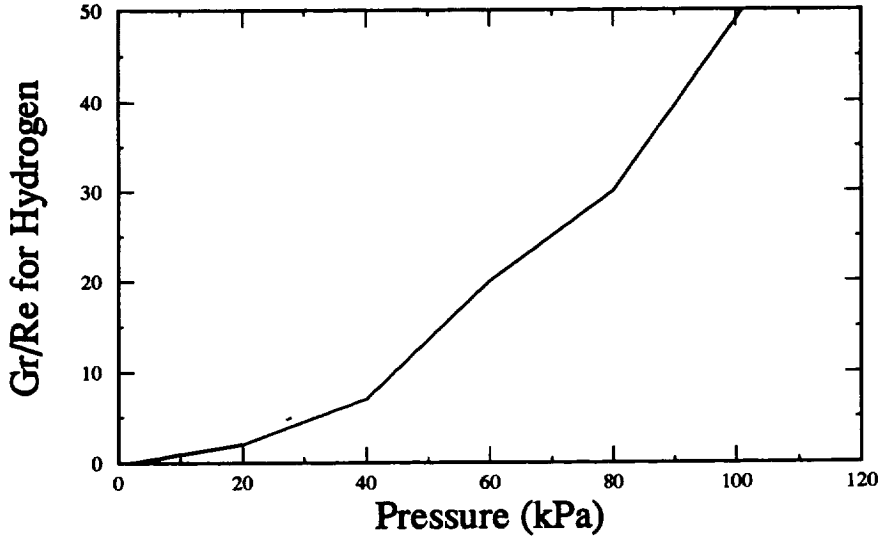
Gr/Re for Hydrogen
50
40
30
20
10
0
0
20
40
60
80
100
120
Pressure (kPa)

Figure 3

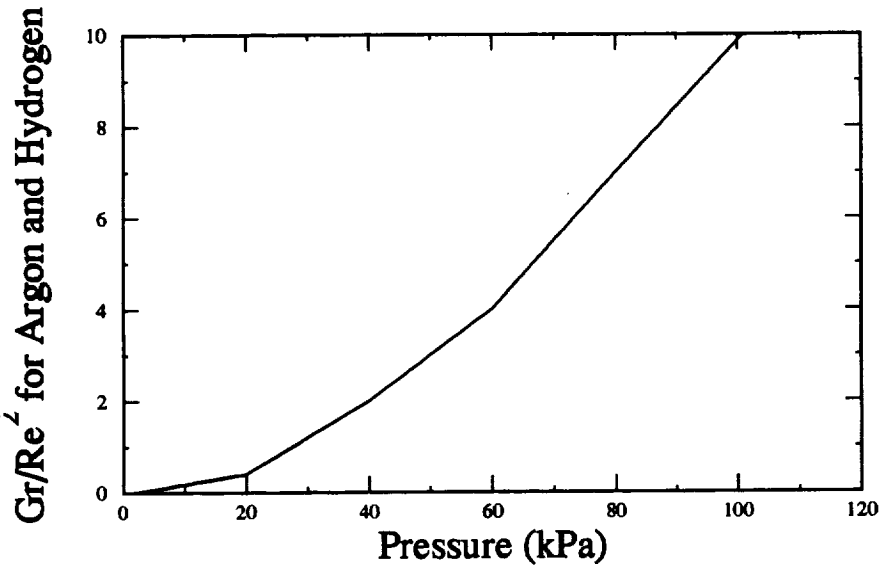
Gr/Re^2 for Argon and Hydrogen
0
2
4
6
8
10
0
20
40
60
80
100
120
Pressure (kPa)

Figure 4

a)

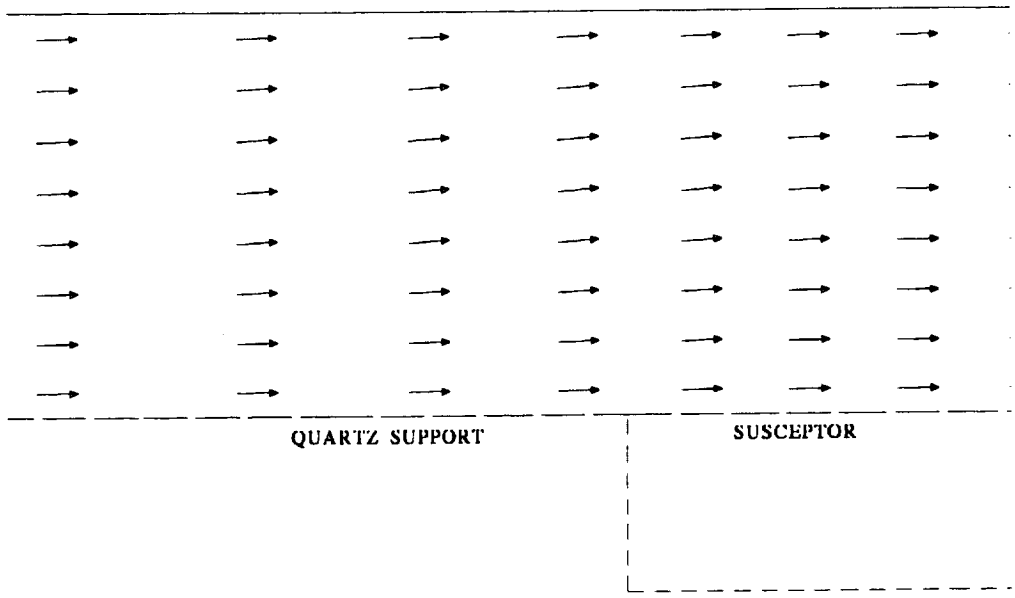

b)

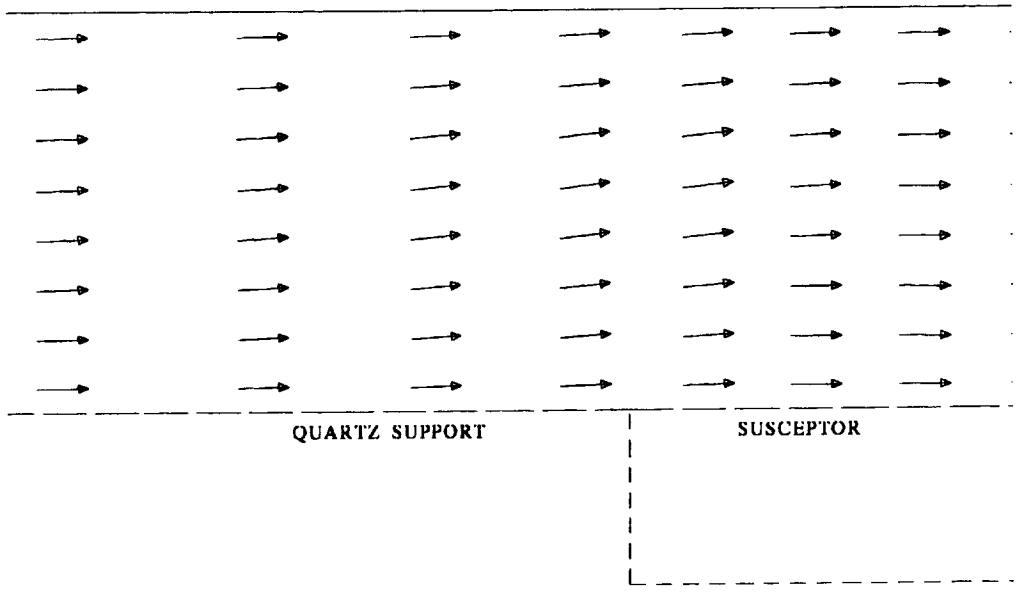

Figure 5

a)

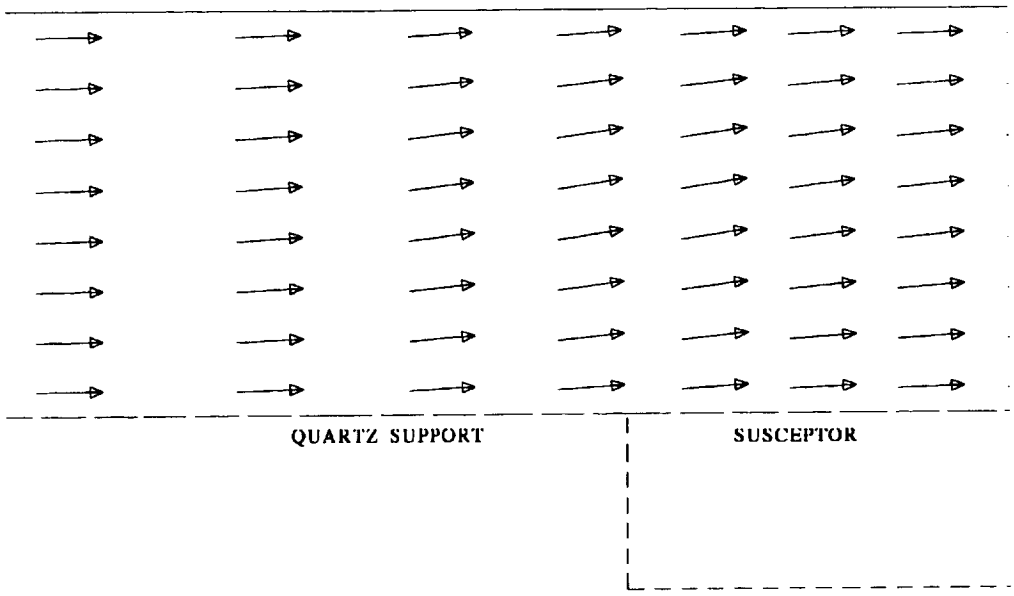

b)

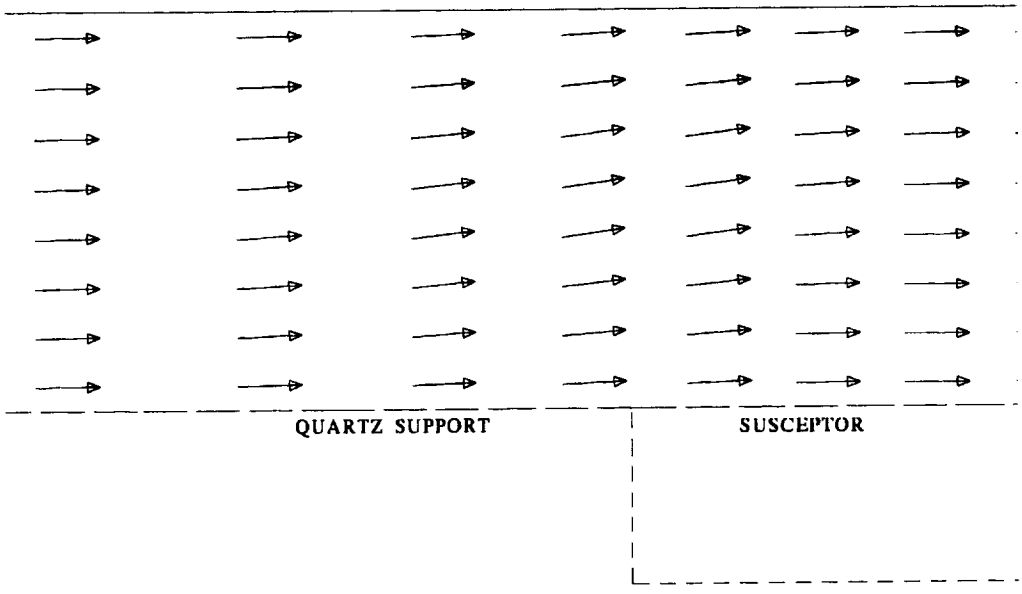

Figure 6

a)

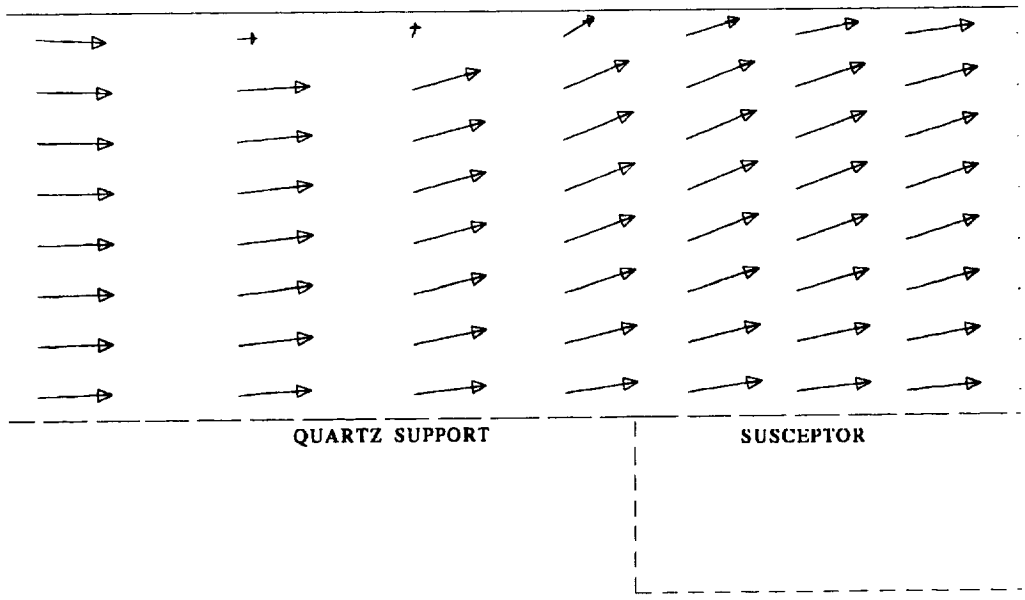

b)

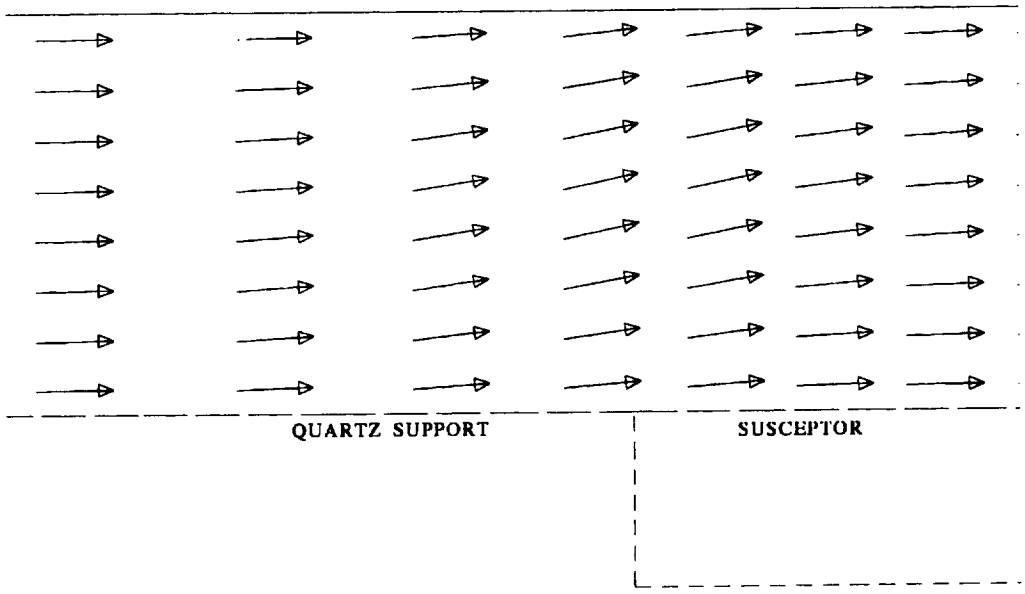

Figure 7

a)

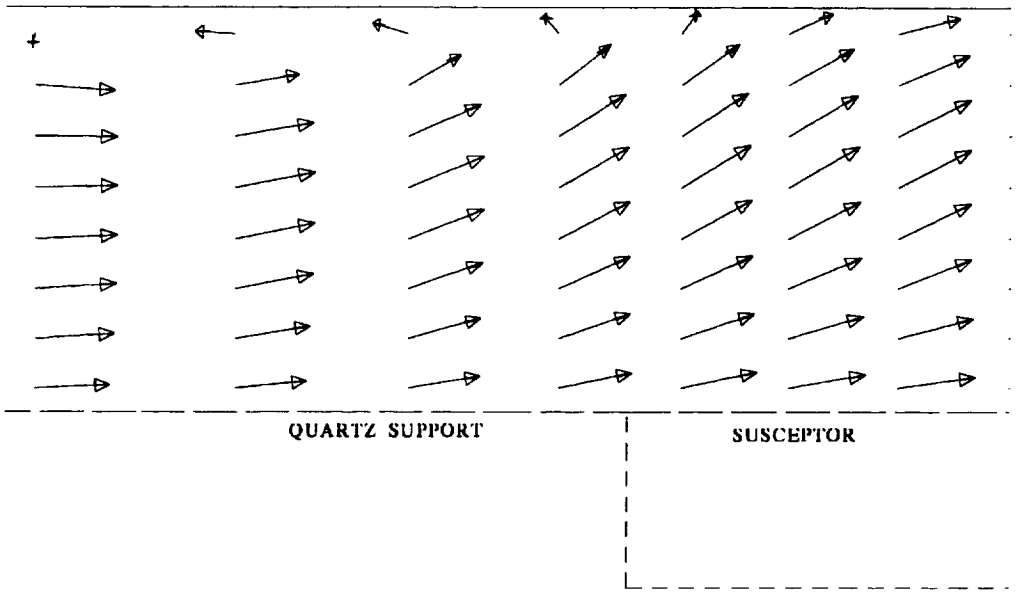

b)

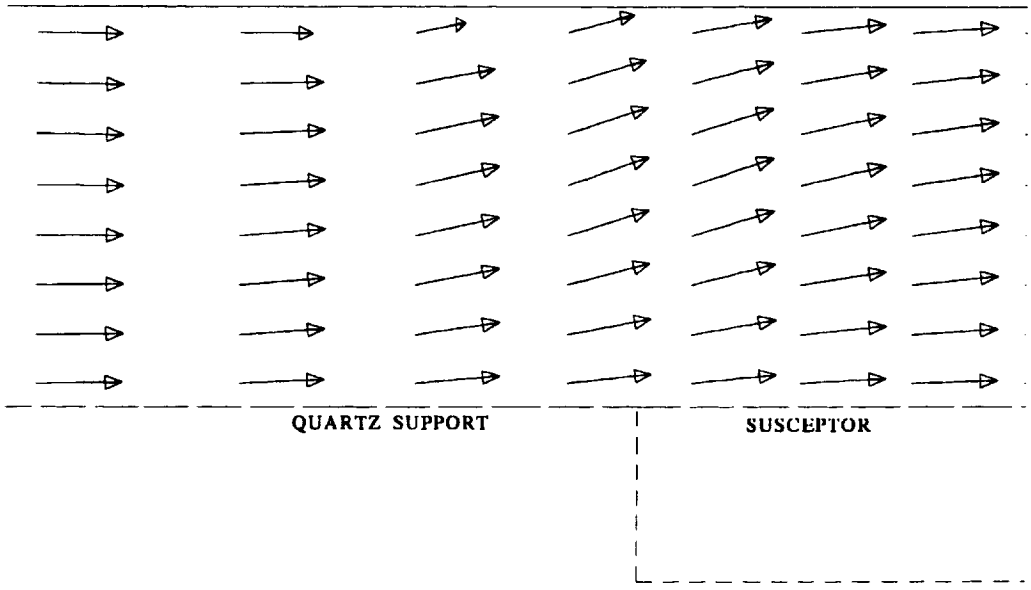

Figure 8

a)

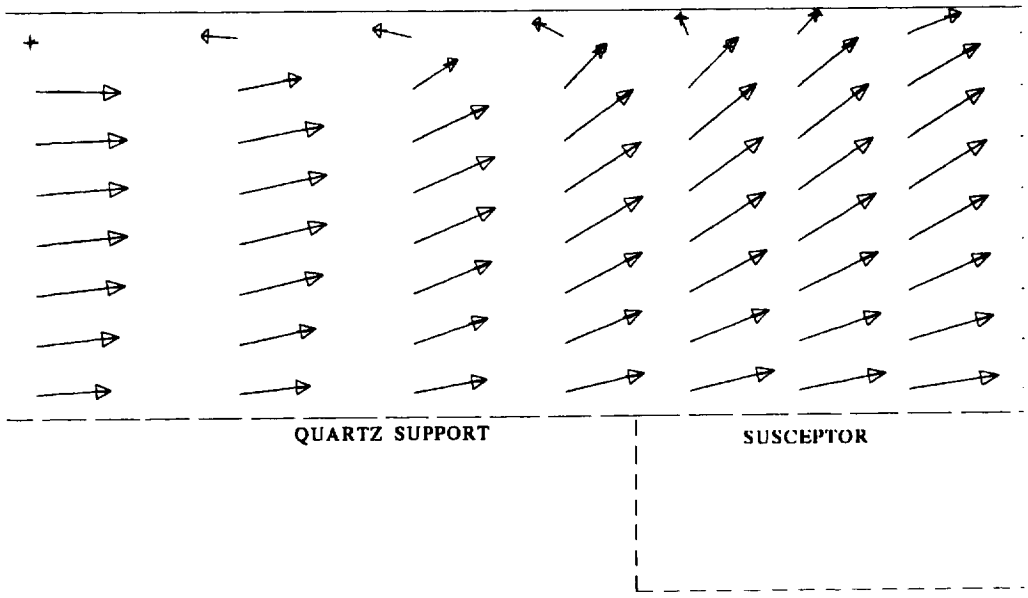

b)

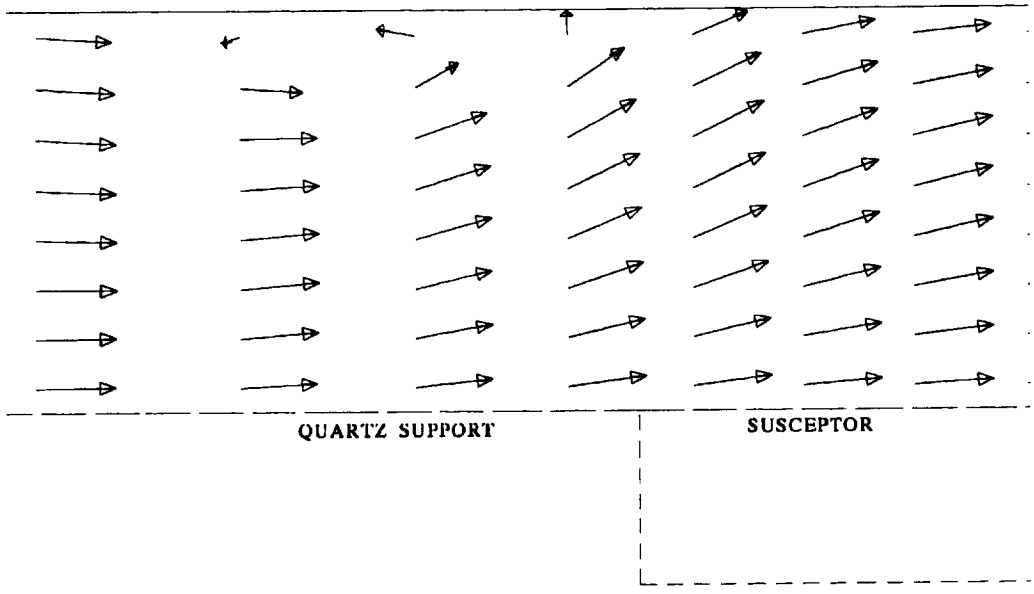

Figure 9

a)

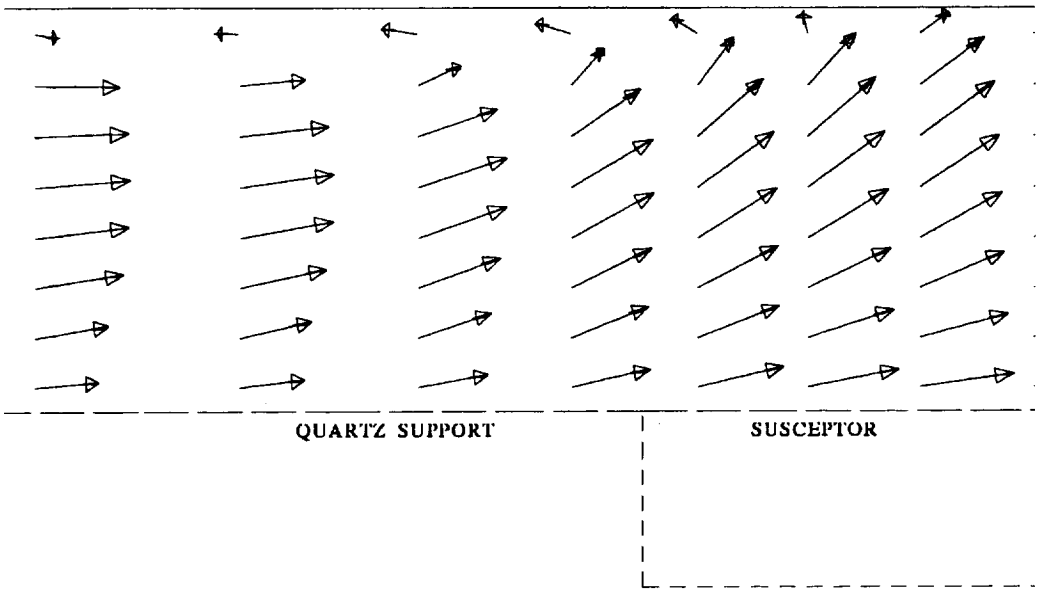

b)

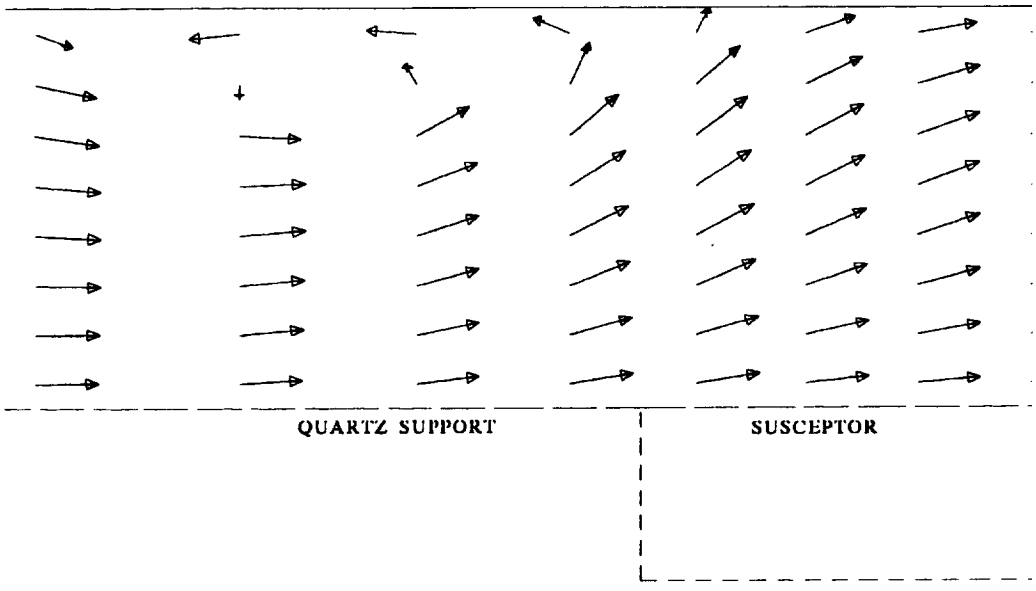

Figure 10

a)

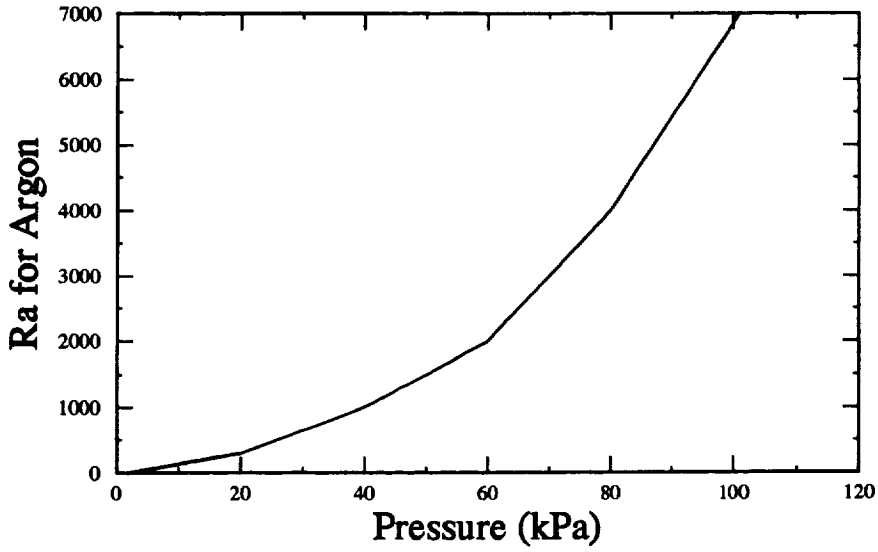
Ra for Argon
7000
6000
5000
4000
3000
2000
1000
0
0
20
40
60
80
100
120
Pressure (kPa)

b)

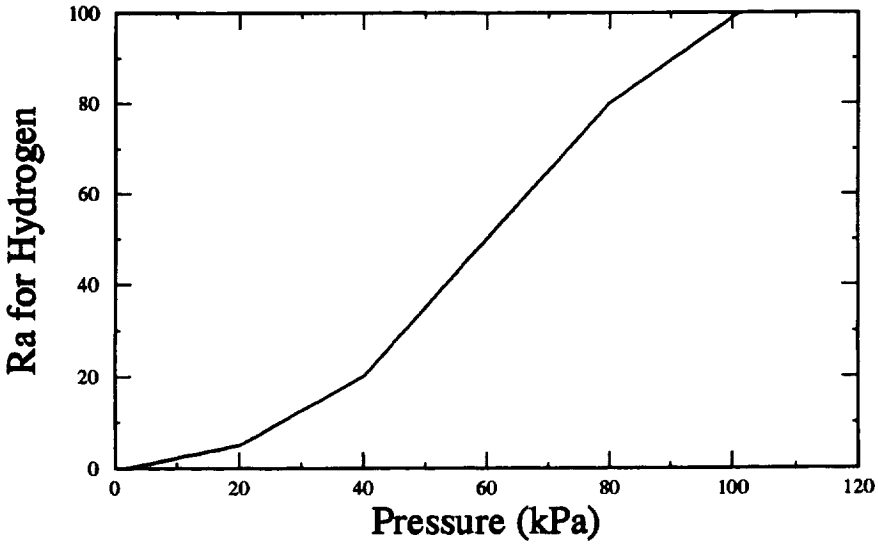
Ra for Hydrogen
100
80
60
40
20
0
0
20
40
60
80
100
120
Pressure (kPa)

Figure 11

a)

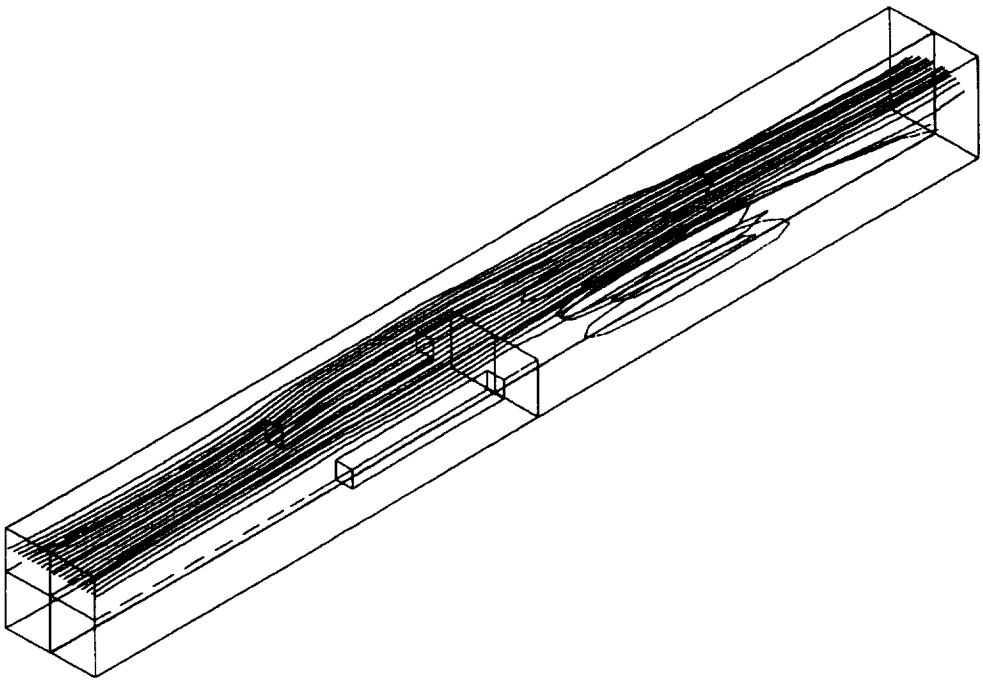

b)

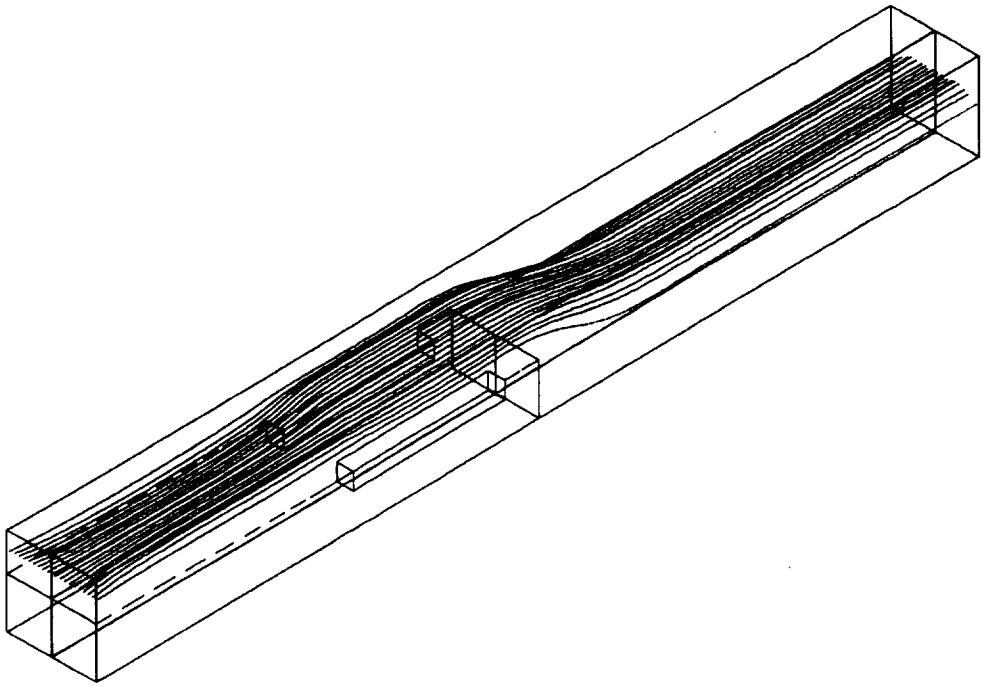

Figure 12

a)

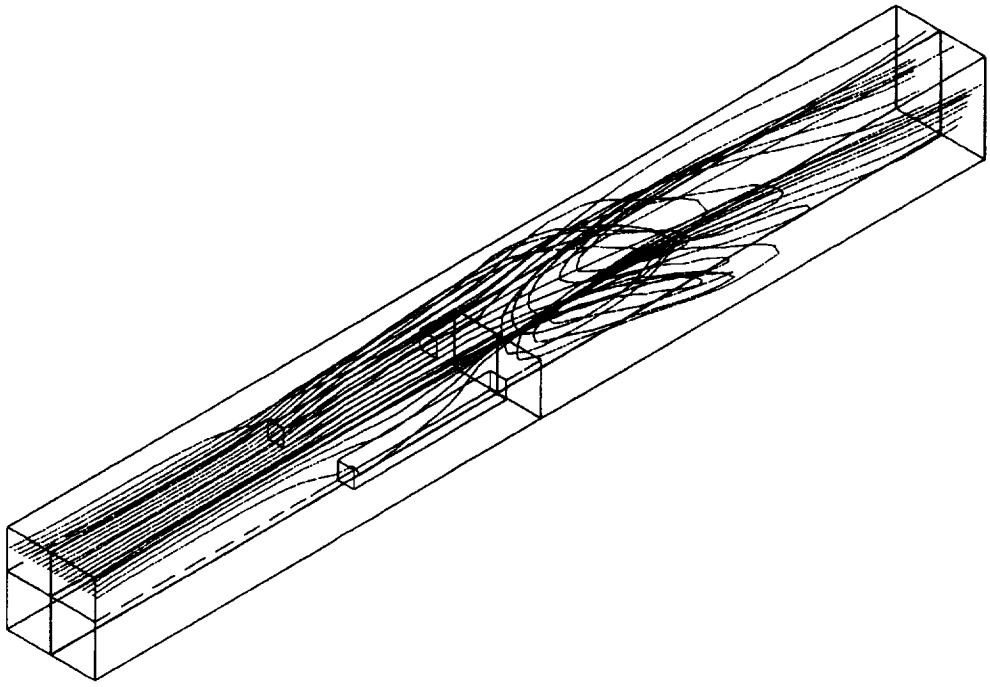

b)

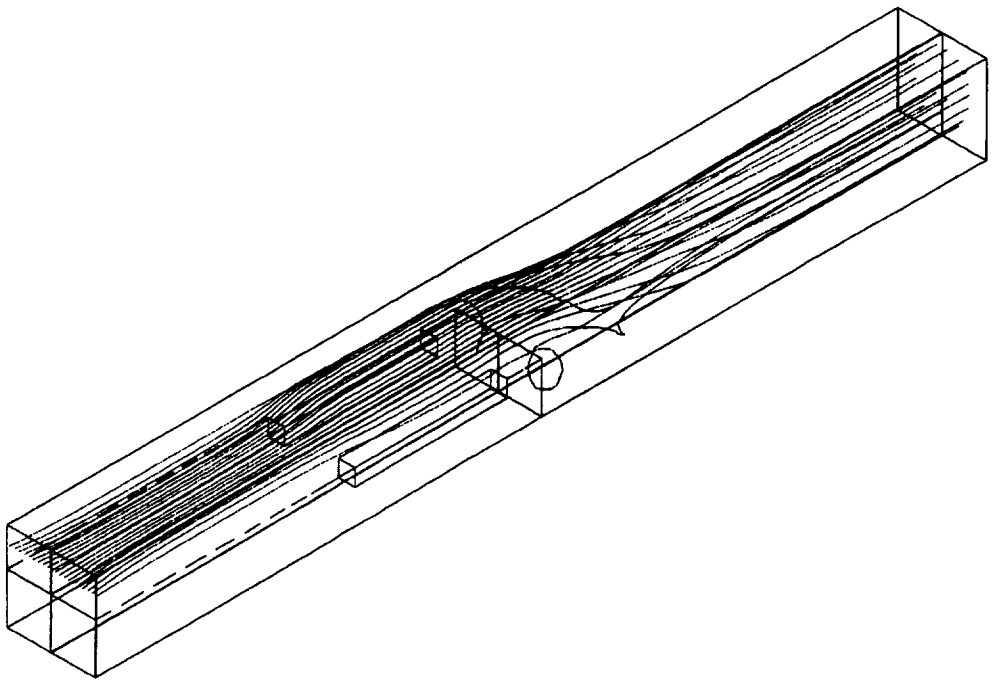

Figure 13

a)

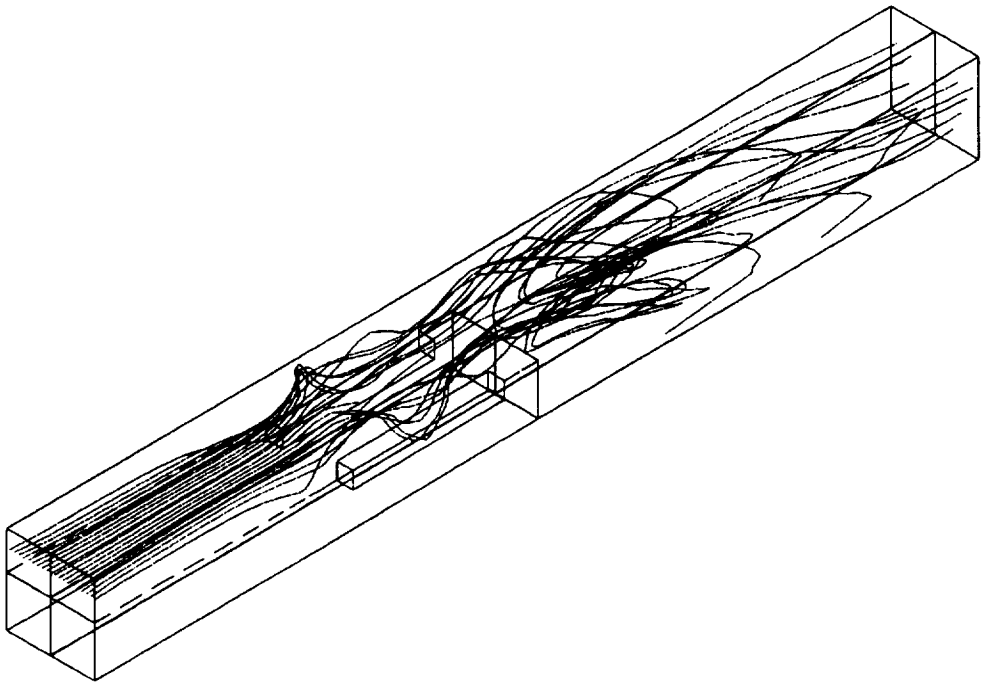

b)

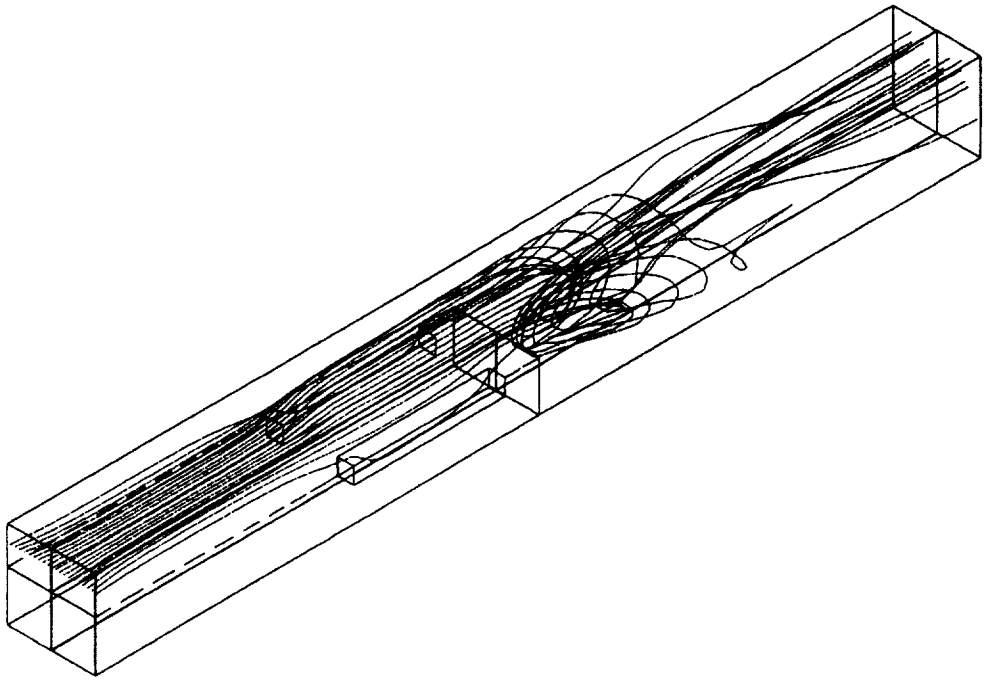

Figure 14

a)

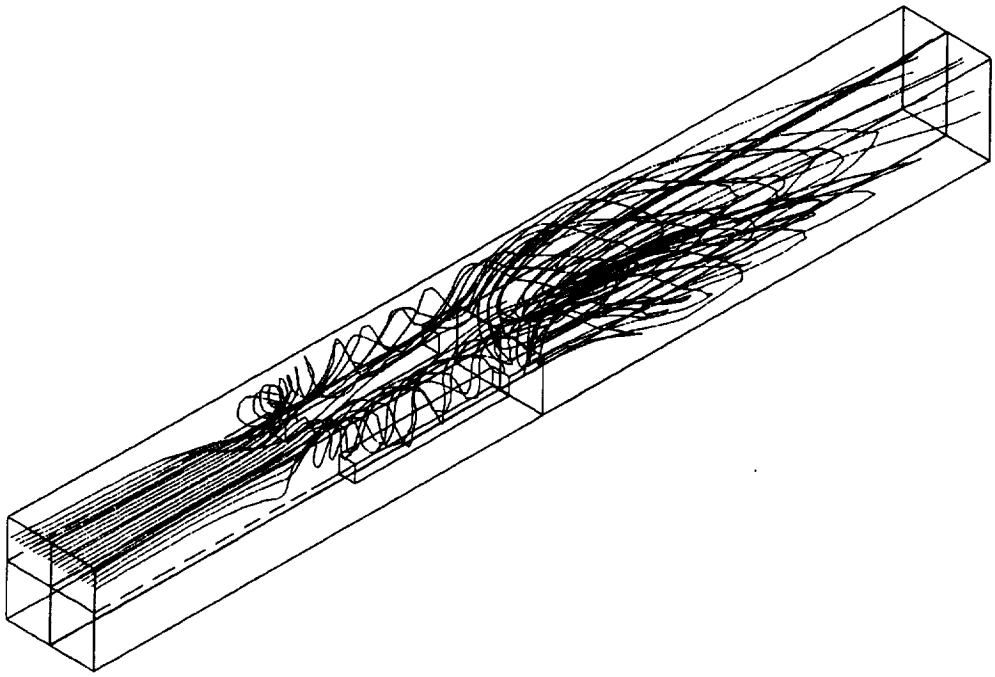

b)

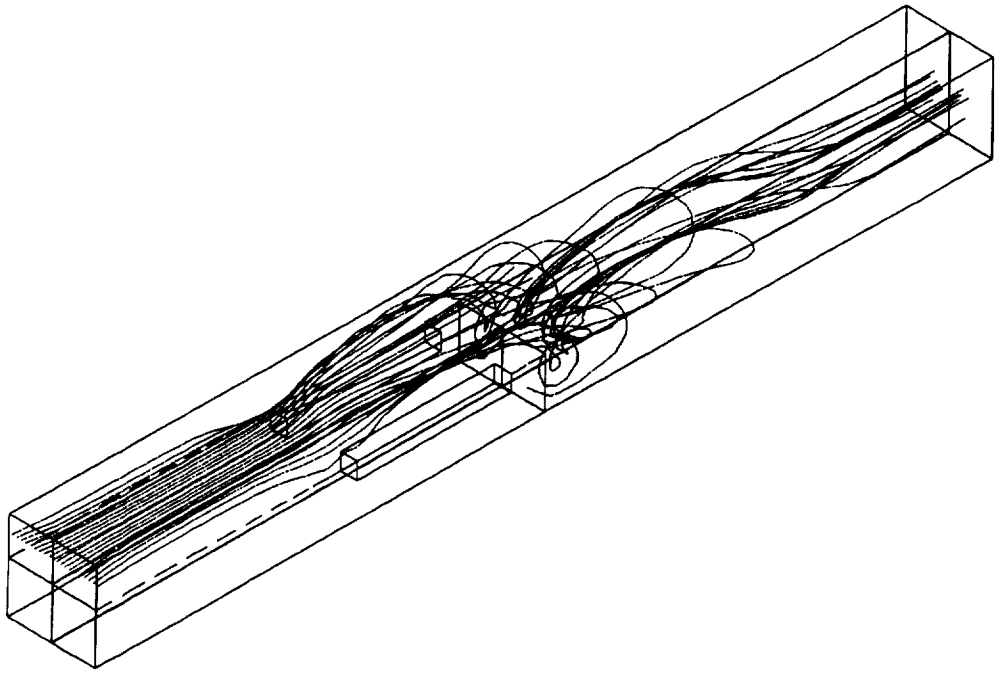

Figure 15

a)

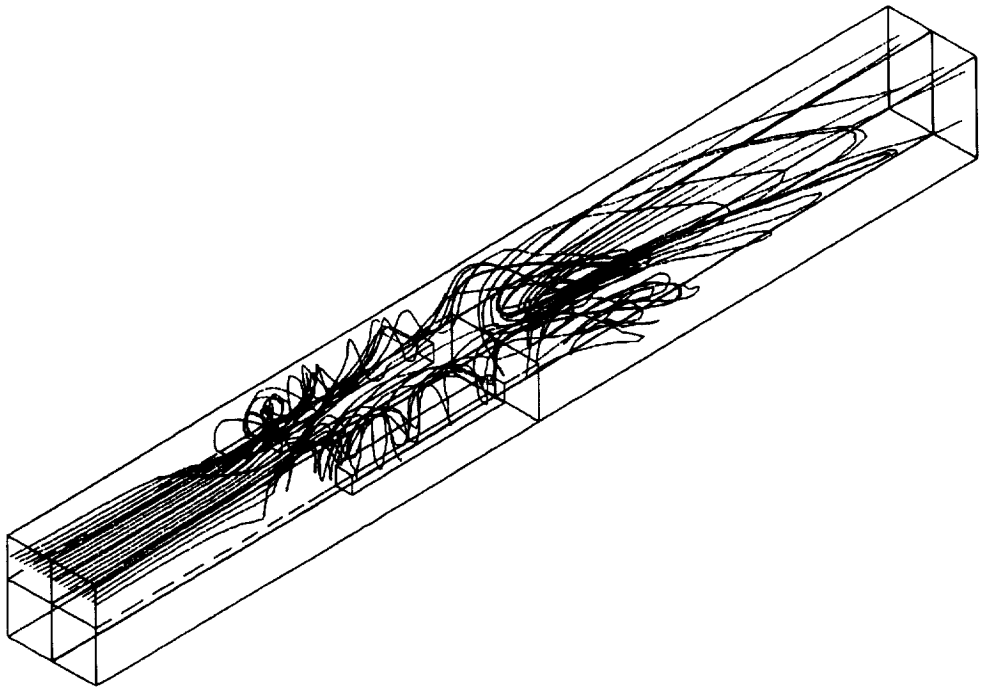

b)

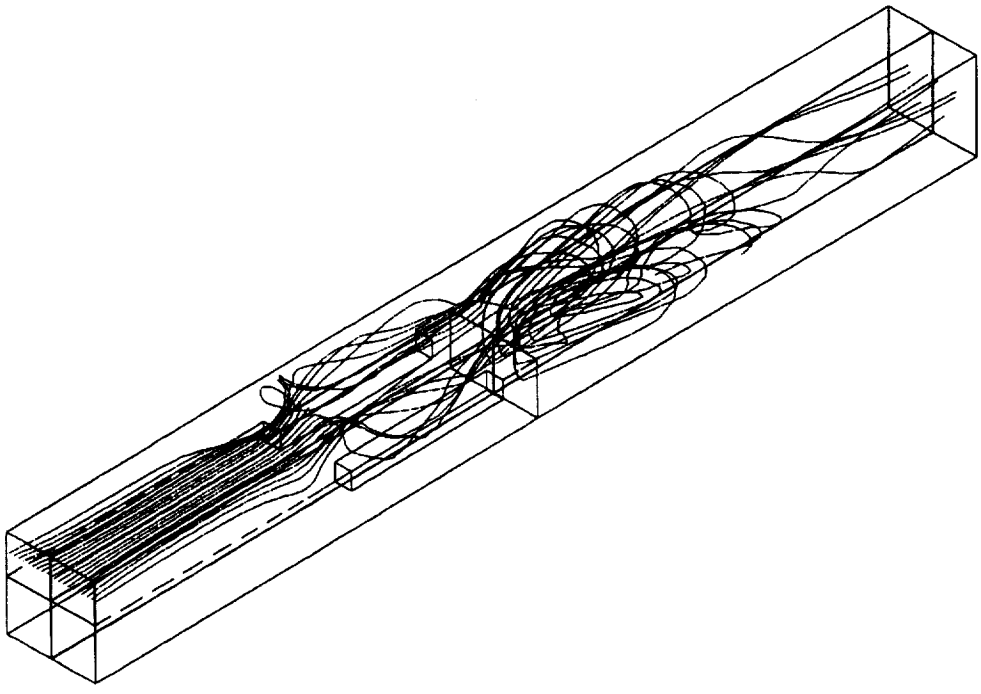

Figure 16

a)

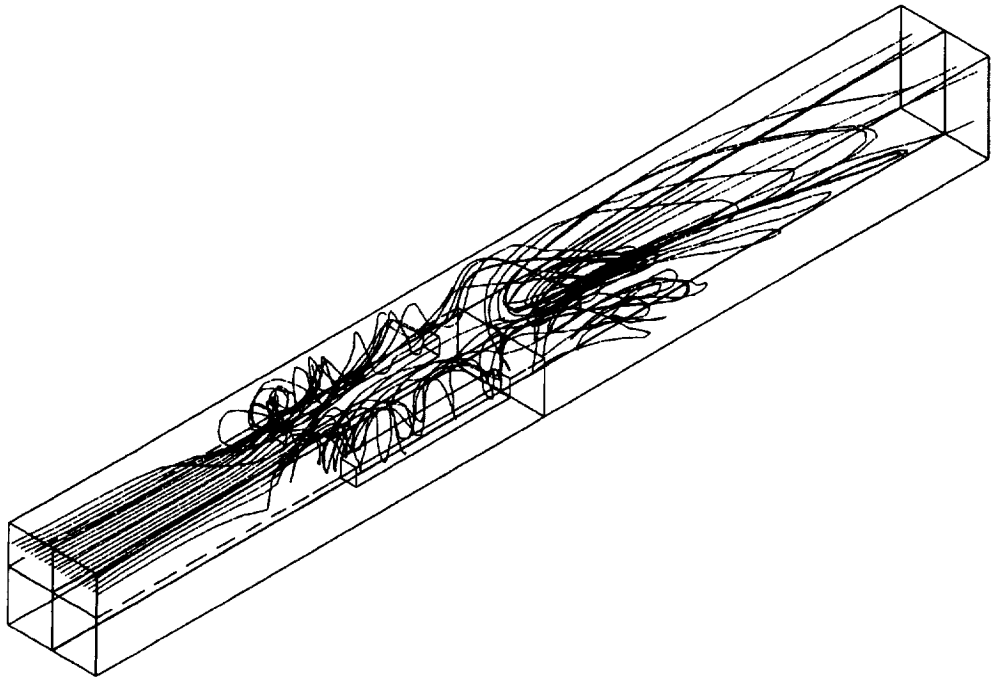

b)

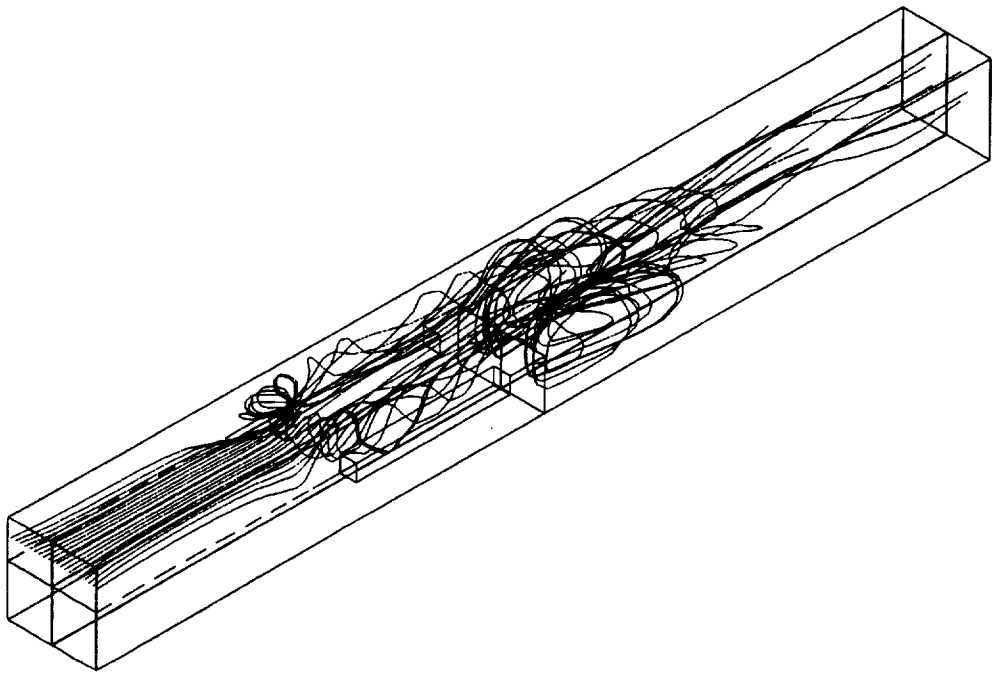

Figure 17